CARDIAC RADIOLOGY

Pictorial essay: Non-coronary applications of cardiac CT

Prabhakar Rajiah

Cardiovascular Imaging Laboratory, Imaging Institute, Cleveland Clinic Foundation, Ohio, United States

Correspondence: Dr. Prabhakar Rajiah, Imaging Institute, Cleveland Clinic Foundation, Ohio, United States. E-mail: radprabhakar@gmail.com

Abstract

Recent advances in scanner technology have enabled computed tomography (CT) scan to evolve into a valuable tool in the noninvasive evaluation of coronary artery disease. Due to its high negative predictive value, CT can act as a gatekeeper, determining which patients require cardiac catheterization. Although mainly used for the evaluation of coronary artery disease, cardiac CT is also useful in the evaluation of various non-coronary cardiac conditions involving the pericardium, pulmonary veins, and the coronary veins and valves, as well as in the assessment of cardiomyopathies, masses, and ventricular and valvular function. This review discusses and illustrates the various non-coronary applications of cardiac CT.

Key words: Cardiac; computed tomography; masses; non-coronary; pericardium; valve

Introduction

Advances in scanner technology have enhanced the ability of computed tomography (CT) scan to evaluate coronary artery disease with a high negative predictive value.[1] Cardiac CT is also increasingly used to evaluate a variety of non-coronary structures including the veins, arteries, chambers, myocardium, valves, and the pericardium. Echocardiography or magnetic resonance imaging (MRI) is the preferred first-line imaging modality for several of these conditions. However, echocardiography is operator dependent and has a limited field-of-view. MRI cannot be used in patients with contraindications, claustrophobia, or those with severe renal dysfunction. CT scan is useful as an alternative imaging tool in these scenarios and may even provide complementary information in some instances.

This review describes and illustrates the non-coronary applications of cardiac CT.

Access this article online	
Quick Response Code:	
	Website: www.ijri.org
	DOI: 10.4103/0971-3026.95403

Veins

Pulmonary veins

Recurrent atrial fibrillation is treated with radiofrequency ablation of the ectopic arrhythmogenic foci located at the veno-atrial junction of the pulmonary veins. Imaging is required prior to this procedure for the evaluation of the pulmonary veins (anatomy, branching pattern, and orientation), left atrial volume, left atrial thrombus, and the relationship of the esophagus to the left atrium. Following the procedure, imaging is required for the detection of complications such as pulmonary stenosis, thrombus, and esophago-atrial fistula.[2] CT scan has a faster turnaround time than MRI. In the electrophysiology lab, the images from volume-rendered 3D CT are combined with electrophysiological data to make an electroanatomic map, which creates a virtual 3D model that is useful for catheter navigation.[3]

Variations in pulmonary venous drainage are seen in 15–20% of the population.[2] In the conjoined pattern, more common on the left, the superior and inferior veins unite to form a single large ostium [Figure 1A], which may make segmental isolation difficult. In the accessory pattern of drainage, accessory, small ostia are seen in addition to the normal four ostia. This is more common in the right middle lobe and the superior segment of the lower lobe.[2] Recognition of accessory veins is essential not only to ensure that these are not inadvertently injured to cause pulmonary stenosis, but also to ensure that all the veins are ablated to avoid recurrence.
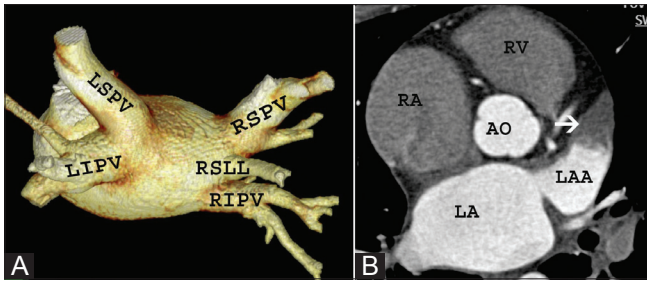
Figure 1 (A, B): Pulmonary vein evaluation. Three-dimensional volume-rendered image (A) shows a common ostium for the left superior pulmonary vein (LSPV) and the left inferior pulmonary vein (LIPV). On the right, in addition to the normal ostia for the right superior pulmonary vein (RSPV) and the right inferior pulmonary vein (RIPV), there is an accessory ostium for the vein draining the superior segment of the right lower lobe (RSLL). Axial CT scan (B) in a patient with atrial fibrillation shows a hypodense lesion in the left atrial appendage (arrow), consistent with a thrombus. LA – left atrium, RA – right atrium, LAA – left atrial appendage, RV – right ventricle, AO – aorta

An early branch is located within 5 mm of the ostium of the main pulmonary vein and is prone for stenosis. Knowledge of the orientation of the veins and the size of the ostia enables determination of catheter size and orientation during the procedure, thus reducing procedure and fluoroscopy times.[4] In **anomalous pulmonary veins,** there is partial or total connection of the pulmonary veins to the systemic veins or the right atrium, resulting in a left-to-right shunt.

Pulmonary venous diameter and area are measured on short axis images. Ablation is difficult and avoided in pulmonary stenosis.[2] The presence of a left atrial thrombus is another contraindication to pulmonary ablation [Figure 1B]. A clear picture of the relationship between the posterior wall of the left atrium/pulmonary veins and the esophagus is essential to avoid creation of an atrio-esophageal fistula.[5]

Coronary veins

The coronary sinus or one of its tributary veins is used as an access route to the left ventricle in various transvenous procedures such as cardiac resynchronization therapy (CRT), percutaneous mitral annuloplasty, and retrograde cardioplegia. If the coronary veins are absent, a transvenous approach is not feasible and surgery may be required. The lateral and posterior cardiac veins may be congenitally absent in 1–3% of the population.[6] The left marginal and posterolateral veins may be absent in as many as 75% of patients with non-ischemic cardiomyopathy.[6,7] A CT venography performed with the same acquisition parameters as a CT angiography, but with a slight delay to capture the venous phase, delineates the coronary venous anatomy [Figure 2]. Delayed contrast-enhanced CT can also detect the presence of extensive scar in the lateral left ventricular wall, which is a predictor of failure of CRT due to the absence of a site for mechanical activation.[7]

Arteries

Lesions in the aorta, pulmonary arteries, and other vessels may be seen incidentally or evaluated using CT scan.
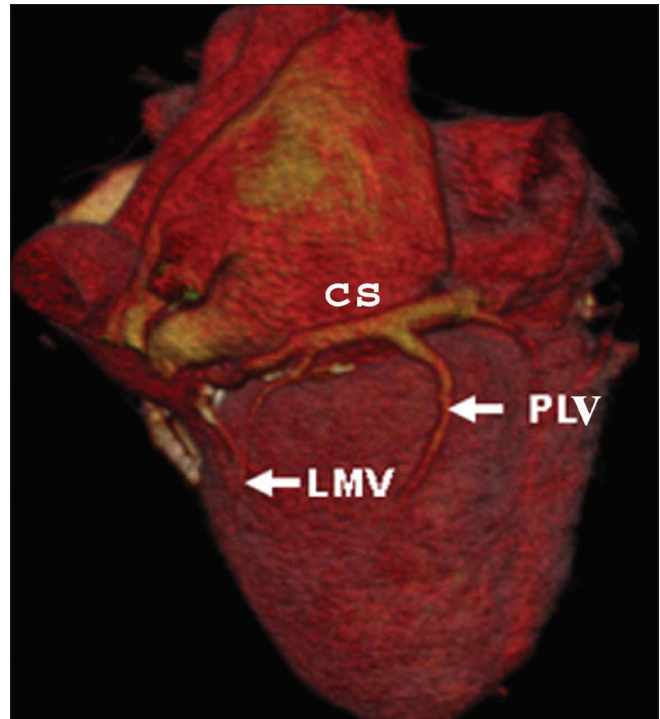

Figure 2: Coronary venous anatomy. Volume-rendered reconstruction of CT cardiac venography shows the coronary sinus (CS) running along the atrioventricular groove. Two tributaries of the CS, namely, the posterolateral vein (PLV) and left marginal vein (LMV), are seen

Aorta

Acute aortic syndrome includes dissection, intramural hematoma, and penetrating atherosclerotic ulcer. **Acute aortic dissection** presents with a flap dividing the vessel into a true and a false lumen. Type A dissection involves the ascending aorta [Figure 3A], warranting surgical management, while Type B involves the arch and descending aorta and can be managed medically in the absence of complications. **Intramural hematoma** presents with high intramural attenuation on a non-contrast scan and with intermediate to high attenuation on a contrast-enhanced scan [Figure 3B].and has similar clinical course as dissection. **Penetrating atherosclerotic ulcer** is more common in the descending thoracic aorta and is seen as focal outpouching of contrast from the aortic lumen. **Aortic dilatation** is diagnosed when the diameter exceeds the normal established value of that particular segment by more than 2 standard deviations (e.g., ascending aorta > 4 cm, descending aorta > 3 cm). **Aortic aneurysm** is diagnosed when the diameter exceeds 1.5 times the normal established value (e.g. ascending aorta > 5 cm, descending aorta > 4 cm). In **aortic coarctation,** there is discrete focal narrowing of the aorta, most commonly seen just distal to the left subclavian artery origin [Figure 3C]. In patients with pulmonary atresia or severe pulmonary stenosis, the lungs are supplied by **major aorto-pulmonary collateral arteries (MAPCAs),** which originate from the aorta or its branches [Figure 3D]. These branches have a disorganized pattern and CT scan

Figure 3 (A–D): Aortic lesions. Axial CT scan (A) shows a flap in the ascending and descending aorta (arrows), consistent with a Type A dissection. Axial CT scan (B) shows a high attenuation intramural lesion in a patient who presented with acute chest pain. Non-contrast CT scan showed high attenuation in the wall (not shown here). The appearances are consistent with intramural hematoma. Sagittal reconstructed CT scan (C) shows a discrete narrowing of the aortic arch (arrow) just beyond the origin of the left subclavian artery, consistent with aortic coarctation. Axial reconstructed MIP image (D) in a patient with history of pulmonary atresia shows a normal left pulmonary artery (LPA). The right pulmonary artery is absent and the right lung is supplied by a major aortopulmonary collateral (MAPCA) originating from the proximal descending thoracic aorta (arrow)

can delineate the exact course of these branches, which is essential for planning surgeries such as unifocalization.

Pulmonary arteries

Pulmonary embolism is seen as a complete or partial intraluminal filling defect in the acute stage [Figure 4A] and as a filling defect, web [Figure 4B], or small caliber vessels in the chronic stage. **Pulmonary artery hypertension** may manifest as a dilated main pulmonary artery (>2.9 cm) [Figure 4C], with features of right ventricular strain such as bowing of the inter-ventricular septum [Figure 4D]. **Pulmonary arteritis** presents with wall thickening and contrast enhancement. **Pulmonary artery tumors** are rare and mimic pulmonary emboli, but cause distension of the artery.

Cardiac Chambers

Masses

CT scan is used in the evaluation of cardiac masses, when MRI is contraindicated. It is ideal in the evaluation of
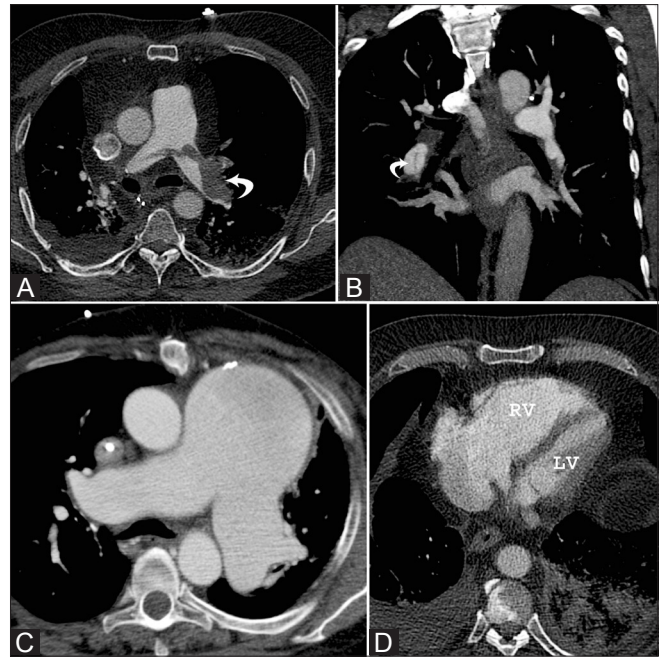

Figure 4 (A–D): Pulmonary artery abnormalities. Axial CT scan (A) shows a large intraluminal filling defect in the left pulmonary artery (arrow) consistent with acute pulmonary embolus. Coronal reformatted CT image (B) shows a linear web in the right interlobar artery, consistent with chronic pulmonary embolus. Axial CT image (C) in a patient with history of recurrent pulmonary embolism shows severely dilated pulmonary arteries, consistent with pulmonary arterial hypertension. Axial CT image (D) in a patient with acute pulmonary embolism and pulmonary hypertension shows dilatation of the right ventricle and bowing of the inter-ventricular septum to the left side, consistent with RV strain

calcifications and in determining arterial supply. **Thrombus** is the most common cardiac mass and is seen as a filling defect, more commonly in the left atrial appendage or in the left ventricle [Figure 5A], adjacent to an infarcted or dyskinetic segment.[8] Thrombus may be confused with slow flow, but it has lower attenuation than slow flow and persists even in delayed phase images, while slow flow disappears. **Lipomatous hypertrophy of the inter-atrial septum** is characterized by a thick, dumb-bell shaped, fatty inter-atrial septum, with sparing of the fossa ovalis [Figure 5B].[9]

Benign neoplasms are more common in the left heart and are typically small with smooth and well-defined margins and no evidence of invasion, feeding vessel, pericardial effusion, or distal metastasis.[9] **Myxoma**, the most common benign neoplasm, is typically seen in the fossa ovalis as a pedunculated mass [Figure 5C]. **Papillary fibroelastoma** is most commonly seen on the cardiac valves. **Hemangioma** may have phleboliths and variable contrast enhancement. **Paraganglioma** shows intense contrast enhancement. **Rhabdomyoma** and **fibroma** are rare pediatric tumors.[9]

Malignant neoplasms are more common in the right heart and typically show ill-defined, infiltrative, and lobulated

margins as well as evidence of invasion of adjacent structures, presence of feeding vessel, pericardial effusion, and distal metastases. **Metastasis** is the most common malignant mass in the heart. Pericardial infiltration is seen as effusion, thickening, or disruption. Myocardial involvement results in thickening and nodularity [Figure 6A]. Primary cardiac **lymphoma** is rare and may present with focal mass, diffuse infiltration, multiple nodules or pericardial effusion. **Angiosarcoma** is the most common type of sarcoma in the heart, with the majority seen in the right atrium [Figure 6B]. **Rhabdomyosarcoma** and **osteosarcoma** are more common in the left atrium. **Leiomyosarcoma, liposarcoma, malignant fibrous histiocytoma,** and **synovial sarcoma** are rare tumors. **Mesothelioma** is a primary malignant tumor of the pericardium, usually associated with asbestos exposure.[9]

Congenital heart disease

MRI is the preferred modality in the evaluation of congenital defects, and CT scan is limited to patients who cannot have an MRI scan. **Atrial septal defects** are classified as ostium primum, ostium secundum [Figure 7A], sinus venosus [Figure 7B], and coronary sinus defects, based on their location in the septum. **Ventricular septal defects** can be membranous, muscular, and inlet or outlet types. Atrioventricular and Gerbode defects can also be seen. A **patent foramen ovale** is seen as a flap in the region of the fossa ovalis, with a left-to-right shunt. CT scan is useful in the morphological evaluation of septal defects prior to percutaneous repair and for the evaluation of complications following the repair.

In **D-transposition of the great arteries**, there is ventriculo-arterial discordance, with the aorta originating from the right ventricle and the pulmonary artery originating from the left ventricle [Figure 8A]. In **congenitally corrected transposition** (L-transposition), there is atrio-ventricular discordance in addition to the ventriculo-arterial discordance, with the left atrium connected to the right ventricle and the right atrium to the left ventricle [Figure 8B, C]. Surgical procedures for treatment of transposition include atrial and arterial switch procedures. **Tetralogy of Fallot** is characterized by right ventricular outflow obstruction, right ventricular hypertrophy, ventricular septal defect, and overriding of aorta. Complete repair [Figure 8D, E] performed in these patients may be complicated by pulmonary regurgitation.[10]

Valves

CT scan has a limited role in the evaluation of valvular abnormalities. It cannot provide flow information obtained with echocardiography or MRI, but can provide morphological information. A bicuspid aortic valve has only two cusps and has a characteristic fish-mouth appearance on short-axis images [Figure 9A] and systolic doming of the anterior leaflet on coronal images. In stenosis, the
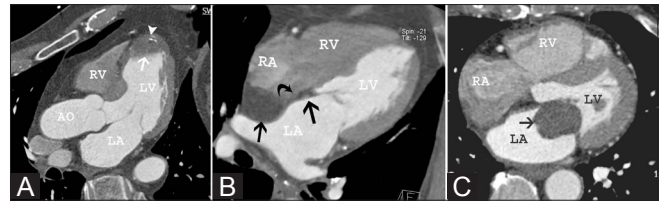

Figure 5 (A–C): Cardiac masses. Three-chamber reformatted CT image (A) shows a layered thrombus in the left ventricular apex (arrow); there is an associated linear band of calcification (arrowhead). Four-chamber reformatted CT image (B) shows a fatty mass in the inter-atrial septum (straight arrows) with sparing of the fossa ovalis (curved arrow); this is characteristic of lipomatous hypertrophy. Axial CT scan (C) shows a well-defined mobile mass (arrow) attached to the anterior mitral valve leaflet, consistent with myxoma
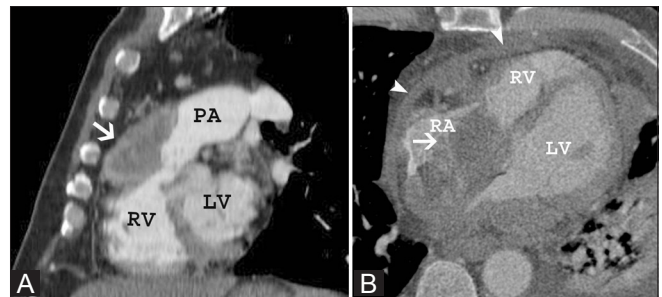

Figure 6 (A, B): Malignant tumors. Sagittal CT image (A) shows a heterogeneous infiltrative mass (arrow) anterior to the right ventricular outflow tract in a patient with prostate carcinoma; this is consistent with metastasis. Axial CT image (B) shows a large irregular mass (arrow) in the right atrium, extending through the tricuspid valve and left ventricle and associated with pericardial thickening and effusion (arrowhead). The mass has also extended into the left atrium
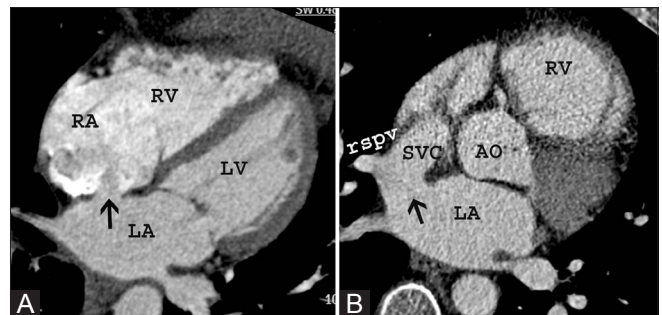

Figure 7 (A, B): Congenital anomalies. Four-chamber CT image (A) shows a defect in the region of the fossa ovalis (arrow), with the contrast jet extending from the left atrium to the right atrium. Axial CT image (B) shows a sinus venosus atrial septal defect (arrow) between the superior vena cava (SVC) and the left atrium (LA). An anomalous pulmonary vein (RSPV) is also seen draining the right upper lobe into the superior vena cava

leaflets are thickened or calcified, with reduced opening during systole in aortic stenosis and during diastole in mitral stenosis [Figure 9B]. The valve area measured by planimetry, both in end-systole and end-diastole, can help quantifying aortic and mitral valve disease.[11] Valve calcification can be qualitatively graded as mild, moderate, or severe, or may be quantified by 3D techniques[12] with
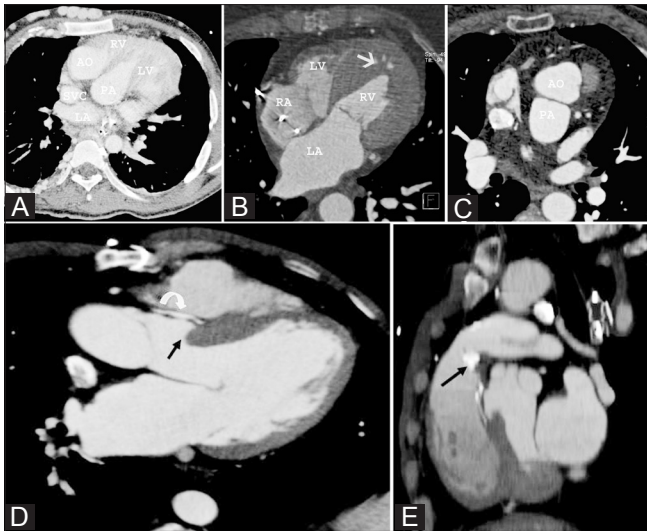
Figure 8 (A–E): Complex congenital anomalies. Four-chamber reconstructed CT image (A) shows the aorta (AO) located anterior and to the right of the pulmonary artery (PA). The aorta originates from the right ventricle (RV) and the pulmonary artery from the left ventricle (LV) in a patient with D-transposition of great arteries. Four-chamber reconstructed CT image (B) shows the left atrium (LA) draining into a hypertrophied morphological RV (systemic ventricle), which opens into the aorta. Moderator band is seen in the RV (arrow). The right atrium (RA) is draining into the morphological LV (pulmonic ventricle), which opens into the pulmonary artery. Axial CT image (C) in the same patient at a higher level shows the aorta located anterior and slightly to the left of pulmonary artery, which is consistent with levotransposition. Three-chamber reconstructed CT image (D) in a patient with repaired tetralogy of Fallot shows a patch repair of the VSD (curved arrow) and partial overriding of the aorta (straight arrow) over the inter-ventricular septum. Sagittal reconstructed CT image (E) in the same patient shows calcified pulmonary conduit (arrow)

Figure 9 (A, B): Valvular lesions. Short-axis CT image (A) through the aortic valve shows a bicuspid valve, with calcification of the leaflet. Four-chamber reconstructed CT image (B) shows severe thickening of the mitral leaflets (arrows) in a patient with mitral stenosis with associated severe left atrial enlargement

Figure 10 (A–C): Prosthetic valve. Short-axis reconstructed CT image (A) shows a tilting disk valve in the mitral position, which is well seated. Short-axis reconstructed CT image (B) shows multiple contrast-filling aortic root abscesses (arrows) surrounding mechanical aortic valve. Coronal-oblique reconstructed CT image (C) in a patient with bioprosthetic aortic valve shows dehiscent valve and pseudoaneurysm (arrow) extending from the left sinus

correlation seen between calcification severity and the severity of aortic stenosis. The size of the regurgitant orifice correlates directly with the grade of regurgitation. Good correlation has been shown between Multidetector CT and echocardiography in the assessment of valve area,[13] valve opening, and regurgitation.[11] Valve motion can be evaluated on retrospective ECG-gated multiphasic cine images. CT scan provides valuable information in patients being evaluated for percutaneous aortic and mitral valve procedures. CT scan is also useful in the evaluation of a prosthetic valve [Figure 10A], which might be challenging with echocardiography and MRI. CT scan can evaluate complications such as thrombus, vegetations, abscess [Figure 10B], pseudoaneurysm [Figure 10C], and valve dehiscence.[14]

Myocardium

Cardiomyopathy

CT scan has a limited role in the evaluation of non-ischemic cardiomyopathies and is used only when there is a contraindication to MRI. CT can help in the characterization of cardiomyopathies based on the morphology and scar pattern. Global ventricular function can be evaluated
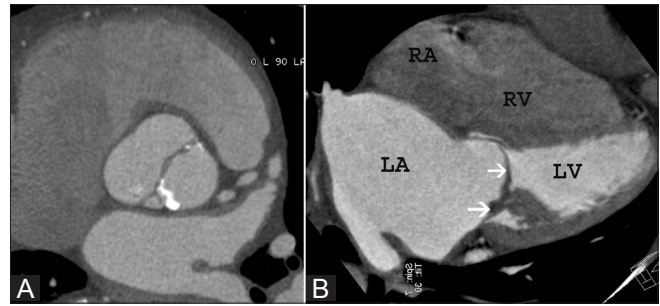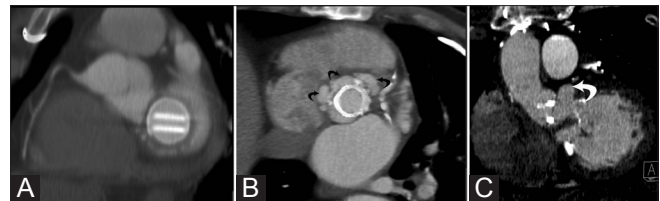
using multiphasic cine images. Regional wall motion can also be evaluated and has shown good correlation with echocardiography.[15]

In **hypertrophic cardiomyopathy**, asymmetric thickening of the myocardium is seen, usually involving the septum [Figure 11A]. CT scan is useful for accurate measurement of the left ventricular thickness and also in evaluating papillary muscle morphology. Patchy contrast enhancement is seen on delayed images due to interstitial fibrosis. **Arrhythmogenic right ventricular dysplasia (ARVD)** is characterized by fibro-fatty replacement of the right ventricular myocardium [Figure 11B]. Other features include right ventricular dilation, right ventricular systolic dysfunction, regional wall-motion abnormalities, and aneurysm. Delayed enhancement may be seen in the fibro-fatty type. In **left ventricular non-compaction**, prominent ventricular trabeculations are seen, with a noncompacted-to-compacted myocardium ratio >2.3:1 in diastole.[16]

CT scan is also useful in the evaluation of ventricular aneurysms, particularly for pre-surgical planning [Figure 11C]. **Aneurysms** have all the three layers and a wide mouth, while **pseudoaneurysms** have only a pericardial lining and a narrow mouth. **Diverticula**
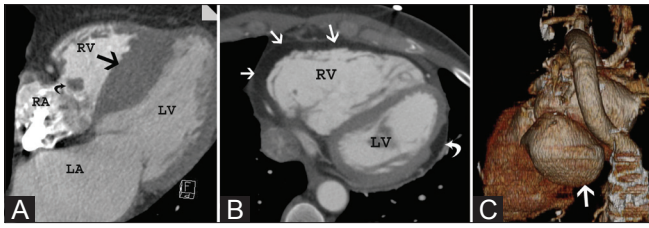
Figure 11 (A–C): Cardiomyopathy. Axial CT image (A) shows asymmetric hypertrophy of the inter-ventricular septum (straight arrow) in a patient with hypertrophic cardiomyopathy. There is also an incidental tricuspid valve fibroelastoma (curved arrow). Axial CT image (B) in a patient who presented with arrhythmia shows diffuse fatty infiltration of the right ventricular myocardium (straight arrows) and dilation of the right ventricle, consistent with arrhythmogenic right ventricular dysplasia (ARVD). There is also focal fatty infiltration of the left ventricle (curved arrow). 3D volume-rendered CT image (C) shows a large pseudoaneurysm (arrow) arising from the base of the left ventricle

Figure 12 (A–C): Pericardial abnormalities. Sagittal reformatted CT image (A) shows a moderate-sized circumferential pericardial effusion (arrows). Axial CT image (B) in a patient with acute pericarditis shows thickening and enhancement of the visceral (straight arrow) and parietal pericardium (curved arrow); there is also surrounding small amount of pericardial fluid (arrowhead). Axial CT image (C) shows extensive calcification of the pericardial layers (arrows). In addition, there is conical deformity of the right ventricle and tubular deformity of the left ventricle, features that are suggestive of pericardial constriction

are usually congenital and usually show synchronous contraction with the ventricles.

Pericardium

CT scan is used in the evaluation of pericardial diseases when assessment of calcification is required or when echocardiography is inconclusive and MRI cannot be performed. **Pericardial effusion** [Figure 12A] is detected with greater sensitivity on CT scan than echocardiography, particularly those that are loculated. Small effusions accumulate adjacent to the posterolateral left ventricular wall, while moderate effusions accumulate anterior to the right ventricle and larger effusions are seen anterior to both the right atrium and the right ventricle. Exudative effusions have higher attenuation than simple effusions. **Cardiac tamponade** may present with deformation and compression of the cardiac chambers, angulation of the inter-ventricular septum, and distension of the superior vena cava/inferior vena cava and reflux of contrast into the inferior vena cava/azygos vein. Cine images show collapse of the right ventricular free wall in early diastole, collapse of the right ventricular free wall during late diastole or early systole, septal rocking, sigmoid septum, and exaggerated respiratory variation of cardiac inflow.[17]

In **acute pericarditis,** there is diffuse or focal pericardial thickening (>4 mm), usually associated with pericardial effusion and contrast enhancement [Figure 12B]. In **chronic inflammatory pericarditis,** the pericardium is irregularly thickened, with or without mild effusion. In **chronic fibrotic pericarditis,** the pericardium is thickened and calcified [Figure 12C]. Calcification in the presence of symptoms is suggestive of pericardial constriction. Other signs of **pericardial constriction** are tubular or conical ventricles [Figure 10C], sigmoid septum, enlarged atria, narrow atrio-ventricular groove, dilated superior vena cava/inferior vena cava/hepatic vein, and pleural effusions. Cine images show diastolic septal bounce, abrupt cessation of diastolic filling, and exaggerated inspiratory septal flattening/reversal and
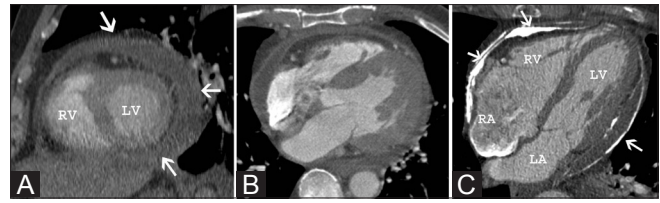
tethering. Occasionally, constriction may be seen without pericardial thickening.[18,19]

Conclusion

Cardiac CT is increasingly being used in the evaluation of various non-coronary disease processes. CT scan is particularly useful when echocardiography is inconclusive and MRI cannot be performed due to contraindications or claustrophobia. CT scan is the ideal modality for the evaluation of calcification.

References

1. Schroeder S, Achenbach S, Bengel F, Burgstahler C, Cademartiri F, de Feyter P, et al. Cardiac computed tomography: Indications, applications, limitations, and training requirements: Report of a Writing Group deployed by the Working Group Nuclear Cardiology and Cardiac CT of the European Society of Cardiology and the European Council of Nuclear Cardiology. Eur Heart J 2008;29:531-56.
2. Cronin P, Sneider MB, Kazerooni EA, Kelly AM, Scharf C, Oral H, et al. MDCT of the left atrium and pulmonary veins in planning radiofrequency ablation for atrial fibrillation: A how-to guide. AJR Am J Roentgenol 2004;183:767-78.
3. Maksimovic R, Dill T, Ristic AD, Seferovic PM. Imaging in percutaneous ablation for atrial fibrillation. Eur Radiol 2006;16:2491-504.
4. Martinek M, Nesser HJ, Aichinger J, Boehm G, Purerfellner H. Impact of integration of multislice computed tomography imaging into three dimensional electroanatomic mapping in clinical outcomes, safely and efficacy using radiofrequency ablation for atrial fibrillation. Pacing Clin Electrophysiol 2007;30:1215-23.
5. Daoud EG, Hummel JD, Houmsse M, Hart DT, Weiss R, Liu Z, et al. Comparison of computed tomographic imaging with intraprocedural contrast esophagogram. Implications for catheter ablation of atrial fibrillation. Heart Rhythm 2008;5:975-80.
6. Van de Veire NR, Schuijf JD, De Sutter J, Schuijf JD, Bleeker GB, Wijffels MC, et al. Non invasive visualization of the cardiac venous system in coronary artery disease patients using 64 slice computed tomography. J Am Coll Cardiol 2006;48:1832-8.
7. Boonyasirinant T, Rajiah P, Schoenhagen P, Halliburton SS, Flamm SD. Relationship of coronay sinus tributaries with myocardial

infarction in ischemic versus non ischemic cardiomyopathy; A comprehensive MDCT assessment with implications for cardiac resynchronization therapy. J Comput Assist Tomogr 2009;3:S23-4.

8. Kim DH, Choi S, Choi JA, Chang JH, Choi DJ, Lim C, *et al*. Various findings of cardiac thrombi on MDCT and MRI. J Comput Assist Tomogr 2006;30:572-7.

9. Rajiah P, Kanne JP, Kalahasti V, Schoenhagen P. Computed tomography of cardiac and paracardiac masses. J Cardiovasc Comput Tomogr 2011;5:16-29.

10. Spevak PJ, Johnson PT, Fishman EK. Surgically corrected congenital heart disease: Utility of 64-MDCT. AJR Am J Roentgenol 2008;191:854-61.

11. Tops LF, Krishnan SC, Schuijf JD, Schalij MJ, Bax JJ. Noncoronary applicatiosn of cardiac multidetector row tomography. J Am Coll Cardiol Imaging 2008;1:94-106.

12. Morgan-Hughes GJ, Owens PE, Roobottom CA, Marshall AJ. Three dimensional volume quantification of aortic valve calcification using multislice computed tomography. Heart 2003;89:1191-4.

13. Feuchtner GM, Müller S, Bonatti J, Schachner T, Velik-Salchner C, Pachinger O, *et al*. Sixty-four slice CT evaluation of aortic stenosis using planimetry of the aortic valve area. AJR Am J Roentgenol 2007;189:197-203.

14. Abbara S, Soni AV, Cury RC. Evaluation of cardiac function and valves by multidetector row computed tomography. Semin Roentgenol 2008;43:145-53.

15. Henneman MM, Bax JJ, Schuijf JD, Jukema JW, Holman ER, Stokkel MP, *et al*. Global and regional left ventriclular function: A comparison between gated SPECT, 2D echocardiography and multi-slice computed tomography. Eur J Nucl Med Mol Imaging 2006;33:1452-60.

16. Williams TJ, Manghat NE, McKay-Ferguson A, Ring NJ, Morgan-Hughes GJ, Roobottom CA. Cardiomyopathy: Appearances on ECG-gated 64-detector row computed tomography. Clin Radiol 2008;63:464-74.

17. Restrepo CS, Lemos DF, Lemos JA, Velasquez E, Diethelm L, Ovella TA, *et al*. Imaging findings in cardiac tamponade with emphasis on CT. Radiographics 2007;27:1595-610.

18. Wang ZJ, Reddy GP, Gotway MB, Yeh BM, Hetts SW, Higgins CB. CT and MR imaging of pericardial disease. Radiographics 2003;23 Spec No:S167-80.

19. Rajiah P, Kanne JP. Computed tomography of pericardium and pericardial abnormalities. J Cardiovasc Comput Tomogr 2010;4: 3-18.

Staying in touch with the journal

1) **Table of Contents (TOC) email alert**
    Receive an email alert containing the TOC when a new complete issue of the journal is made available online. To register for TOC alerts go to **www.ijri.org/signup.asp.**

2) **RSS feeds**
    Really Simple Syndication (RSS) helps you to get alerts on new publication right on your desktop without going to the journal's website. You need a software (e.g. RSSReader, Feed Demon, FeedReader, My Yahoo!, NewsGator and NewzCrawler) to get advantage of this tool. RSS feeds can also be read through FireFox or Microsoft Outlook 2007. Once any of these small (and mostly free) software is installed, add **www.ijri.org/rssfeed.asp** as one of the feeds.